Differential depletion of GluN2A induces heterogeneous schizophrenia-related phenotypes in mice

Yi Lu,[a,b,f] Longyu Mu,[a,b,f] Justin Elstrott,[c] Chaoying Fu,[a] Cailu Sun,[a,b] Tonghui Su,[a,b] Xiaofan Ma,[d] Jia Yan,[d] Hong Jiang,[d] Jesse E. Hanson,[e] Yang Geng,[a,**] and Yelin Chen[a,g,*]

[a]Interdisciplinary Research Centre on Biology and Chemistry, Shanghai Institute of Organic Chemistry, Chinese Academy of Sciences, No.100 Haike Rd., Pudong New District, Shanghai 201210, China
[b]University of Chinese Academy of Sciences, Beijing 100049, China
[c]Department of Translational Imaging, Genentech Inc., South San Francisco, CA 94080, USA
[d]Department of Anaesthesiology, Shanghai Jiao Tong University School of Medicine Affiliated Ninth People's Hospital, Shanghai 200011, China
[e]Department of Neuroscience, Genentech Inc., South San Francisco, CA 94080, USA

eBioMedicine
2024;102: 105045
Published Online xxx
https://doi.org/10.1016/j.ebiom.2024.105045

Summary

Background Schizophrenia, a debilitating psychiatric disorder, displays considerable interindividual variation in clinical presentations. The ongoing debate revolves around whether this heterogeneity signifies a continuum of severity linked to a singular causative factor or a collection of distinct subtypes with unique origins. Within the realm of schizophrenia, the functional impairment of GluN2A, a subtype of the NMDA receptor, has been associated with an elevated risk. Despite GluN2A's expression across various neuronal types throughout the brain, its specific contributions to schizophrenia and its involvement in particular cell types or brain regions remain unexplored.

Methods We generated age-specific, cell type-specific or brain region-specific conditional knockout mice targeting GluN2A and conducted a comprehensive analysis using tests measuring phenotypes relevant to schizophrenia.

Findings Through the induction of germline ablation of GluN2A, we observed the emergence of numerous schizophrenia-associated abnormalities in adult mice. Intriguingly, GluN2A knockout performed at different ages, in specific cell types and within distinct brain regions, we observed overlapping yet distinct schizophrenia-related phenotypes in mice.

Interpretation Our interpretation suggests that the dysfunction of GluN2A is sufficient to evoke heterogeneous manifestations associated with schizophrenia, indicating that GluN2A stands as a prominent risk factor and a potential therapeutic target for schizophrenia.

Funding This project received support from the Shanghai Municipal Science and Technology Major Project (Grant No. 2019SHZDZX02) awarded to Y.C. and the Natural Science Foundation of Shanghai (Grant No. 19ZR1468600 and 201409003800) awarded to G.Y.

Keywords: NMDA receptor; GluN2A; Schizophrenia; Conditional knockout mouse; Medial prefrontal cortex; Excitatory synaptic transmission

Introduction

Schizophrenia, a disabling psychiatric disorder with a global prevalence of approximately 1%,[1] is characterized by a high recurrence rate and typically manifests with positive, negative, and cognitive deficits during late adolescence or early adulthood.[2,3] This complex neuropsychiatric syndrome exhibits notable interindividual variation in clinical manifestations, genetic factors, neurobiological characteristics, and phenotypic profiles, rendering it a heterogeneous disease.[4–6] The dysfunction of the dopaminergic system has been implicated in positive symptoms but not negative symptoms and cognitive deficits.[7–9]

*Corresponding author.
**Corresponding author.
E-mail addresses: chenyelin@sioc.ac.cn (Y. Chen), gengyang@sioc.ac.cn (Y. Geng).
[f]Contributed equally.
[g]Lead Contact: Yelin Chen, chenyelin@sioc.ac.cn, tel: 086-21-68582361.

Research in context

Evidence before this study

Schizophrenia is a heterogeneous disease which exhibits notable interindividual variation in clinical manifestations. Recent studies have highlighted that hypofunction of the glutamatergic system, particularly the NMDA type of glutamate receptor (NMDAR), can induce all schizophrenia-associated symptoms, raising the possibility of a common underlying factor contributing to the diverse symptomatology. Notably, recent large-scale human genetic studies have only identified rare variants in *Grin2a* (the gene encoding GluN2A, a subtype of the NMDA receptor) resulting in loss of GluN2A function as being associated with schizophrenia risk.

Added value of this study

Our study reveals that germline ablation of GluN2A can induce various schizophrenia-associated abnormalities in adult mice. Mechanistically we report overlapping yet distinct schizophrenia-related phenotypes in mice based on the timing of GluN2A knockout, the involvement of specific cell types, and targeting distinct brain regions.

Implications of all the available evidence

Our findings demonstrate that GluN2A makes specific contributions to schizophrenia from particular cell types or brain regions. The observed dysfunction of GluN2A is sufficient to elicit the heterogeneous manifestations associated with schizophrenia. Considering its role, GluN2A emerges as a potential therapeutic target for schizophrenia, emphasizing the importance of early intervention.

A subgroup of non-competitive NMDAR antagonists, including phencyclidine (PCP) and ketamine, triggers behaviours resembling all three symptom categories of schizophrenia (positive, negative, and cognitive) in human subjects.[10,11] These findings collectively support the NMDAR hypofunction hypothesis, suggesting that reduced NMDAR activity may underlie all symptoms of schizophrenia.

The glutamatergic system, particularly the NMDA type of glutamate receptor (NMDAR), plays a significant role in schizophrenia. Transient inhibition of NMDAR can induce schizophrenia-related symptoms in healthy individuals and exacerbate symptoms in patients with schizophrenia.[12,13] Moreover, patients with autoantibodies targeting NMDARs present with encephalitis and psychosis.[14] Human genetic studies have linked partial loss of NMDAR function to an increased risk of schizophrenia.[15,16] Functional NMDARs are tetramers comprising two obligatory GluN1 subunits and two GluN2 or GluN3 subunits.[17] Broad NMDAR inhibition or genetic ablation of GluN1 in mice leads to behavioural abnormalities associated with schizophrenia.[18–21]

NMDAR subtypes exhibit diversity in their expression patterns and functional properties.[17] Within the schizophrenia-associated forebrain region, GluN2A and GluN2B are the major GluN2 subunits expressed.[22] GluN2B expression initiates during prenatal development,[22,23] whereas GluN2A expression commences after birth, reaching relatively high levels in various adult brain regions.[17] Selective inhibition or genetic ablation of GluN2B can induce some schizophrenia-related abnormalities,[24–26] supporting its involvement in the disorder. However, recent large-scale human genetic studies have only identified rare variants in *Grin2a* (the gene encoding GluN2A) resulting in the loss of GluN2A function as being associated with schizophrenia risk.[15,16] Additional evidence suggests a potential association between reduced GluN2A expression and schizophrenia.[27–29] GluN2A mutations have also been linked to epilepsy aphasia syndromes.[30,31] Although GluN2A dysfunction is clearly implicated in psychiatric diseases, the precise mechanisms through which GluN2A loss affects brain function and behaviour remain largely unknown.

Numerous hypotheses concerning neural circuits have surfaced to elucidate how diminished NMDAR activity contributes to symptoms of schizophrenia. One such hypothesis posits that cognitive impairments may emanate from diminished NMDAR functions on cortical gamma-aminobutyric acid (GABA) interneurons, particularly fast-spiking parvalbumin (PV) interneurons. The curtailed inhibitory signals from PV + interneurons may disrupt dorsolateral prefrontal cortex (DLPFC) activity synchronization during gamma oscillations, typically associated with working memory function.[32] Thus, the proposal suggests that drugs selectively enhancing the inhibitory impact of PV + interneurons on prefrontal pyramidal neurons could potentially alleviate working memory deficits in individual with schizophrenia. Noteworthy is the widespread distribution of GluN2A in the brain, expressed in diverse neuronal types; however, its specific contributions to schizophrenia from distinct cell types or brain regions remain unexplored.

This study employed germline GluN2A knockout mice to probe GluN2A's role in schizophrenia. Additionally, we generated various GluN2A conditional knockout mouse lines to assess the consequences of GluN2A deficiency on schizophrenia across diverse developmental stages, neuronal subtypes (excitatory and inhibitory neurons), and specific brain regions. Subsequent to these manipulations, we conducted comprehensive investigations to unveil the molecular, electrophysiological, and EEG alterations induced by GluN2A depletion.

Methods

Animals

We housed groups of 3–5 mice per cage in a 12-h light/dark cycle (lights on at 8:00 a.m.) with ad libitum access to food and water. The Grin2a$^{-/-}$ mice (GluN2A knockout, GluN2A KO mice) with constitutive GluN2A deletion were obtained from RIKEN (Rikagaku Kenkyusho/Institute of Physical and Chemical Research) BRC through the National Bio-Resource Project of the MEXT, Japan (Strain name: B6.129S6-Grin2a <tm1Nak>/NakRbrc, BRC No: RBRC01195).[33]

We established a Grin2a$^{fl/fl}$ mouse line, as previously described.[34] Subsequently, we crossbred this line with various Cre recombinase-expressing mouse lines—UBC-CreERT2, NEX-Cre, and vGAT-Cre—to create distinct Grin2a conditional knockout mouse models. UBC-CreERT2$^{+/-}$::Grin2a$^{fl/fl}$ mice were employed to delete GluN2A during different developmental stages via tamoxifen administration. The UBC-CreERT2 mouse strain was obtained from Shanghai Model Organisms Centre, Inc (Shanghai, China). For the deletion of GluN2A in excitatory neurons, we utilized NEX-Cre$^{+/-}$::Grin2a$^{fl/fl}$ mice, and for inhibitory neurons, vGAT-Cre$^{+/-}$::Grin2a$^{fl/fl}$ mice (NEX and vGAT cKO). The NEX-Cre and vGAT-Cre mouse lines were generously gifted by Dr. Zilong Qiu from the Institute of Neuroscience, Chinese Academy of Sciences, and Dr. Ji Hu from ShanghaiTech University, respectively. Both male and female mice were included as study subjects.

All behavioural data were collected between 10 a.m. and 5 p.m. The order of the behavioural tasks was as follows: nest building test, open field test, Y maze, three chamber social test, and prepulse inhibition. Each task was conducted on separate days, with a time interval of 3–7 days between tasks.

Tamoxifen administration

Tamoxifen (TAM, Abcone, T56488) was dissolved in a solution comprising 90% corn oil and 10% ethanol, reaching a concentration of 20 mg/ml. The prepared TAM solution can be stored in a light-proof tube at 4 °C for up to one week. UBC Control/cKO mice were administered intraperitoneal injections of 0.1 ml TAM per mouse daily for a duration of 7 days.

Open field test (OFT)

Mice were acclimated to the testing room for at least 30 min before testing. The luminance within the open field boxes was adjusted to a range of 9–11 lux. Each mouse was placed individually in a 40 × 40 cm box, and their movements were recorded for 1 h using the EthoVision XT 11.5 system (Noldus Information Technology Inc., Leesburg, VA, USA). To eliminate residual odors between trials, the boxes were cleaned with 75% ethanol.

Nest building test (NBT)

Every mouse was individually transferred into a new cage with fresh bedding one day before the experiment. On day 0, a pressed cotton square nestlet (5 × 5 cm, approximately 2 g) was weighed and introduced into each cage 1 h before the dark phase. The quantity of unused nestlet material was documented on days 1, 3, 5, and 7. Great care was taken to minimize any disruption to the mice and their cage environment.

Three-chamber social test (TCST)

Mice acclimated to the testing room for a minimum of 30 min before the initiation of the TCST. The test utilized a three-chambered box (61 × 40 × 22 cm) featuring a central chamber (20 × 40 × 22 cm) and two open lateral compartments (20 × 40 × 22 cm). Individual mouse holders (cylindrical, 12 cm diameter, 9 cm height) were positioned with in the middle of the lateral compartments. The subject mouse underwent three sequential sessions habituation, sociability, and social novelty. During habituation, both holders remained empty. In the sociability session, a stranger 1 (S1) mouse occupied the left holder, while the right holder remained empty.

In the social novelty session, the left holder continued to house the stranger 1 mouse, while a stranger 2 (S2) was introduced into the right holder. Each session lasted 10 min, providing the subject mouse with the opportunity to explore all three compartments. The average time interval between sessions ranged from 2 to 3 min. Social stimulus mice matched the subject mice in terms of age, sex, and strain background and were unfamiliar to the subjects. Cage-mates of the subject mice were deliberately avoided. The EthoVision XT 11.5 system (Noldus Information Technology Inc., Leesburg, VA, USA) recorded and analysed the trace of the subject mouse. Sniffing time was defined as the duration when the mouse's nose was within 3.5 cm of the holder edge. Prior to each round, the chamber and holder were cleaned with 75% ethanol.

Y-maze spontaneous alternation test

The Y-maze spontaneous alternation test employed a Y-shaped maze with three identical arms (30 × 6 × 15 cm), set at a 120° angle apart. The intersecting area was marked as the centre zone. Mice were placed at the end of one arm facing the centre zone and allowed to freely explore the maze for 10 min. Before each trial, the maze underwent cleaning with 75% ethanol. An entry was scored when all four limbs were within an arm. Data collection utilized the EthoVision XT 11.5 system (Noldus Information Technology Inc., Leesburg, VA, USA). Alternation was defined as consecutive entries into three different arms without repetition (e.g., ABC, BCA, CAB … …).

Alternation percentage was calculated as (Alternation/Max Alternation) × 100, where Max Alternation

refers to the maximum possible alternations in a session.

Prepulse inhibition (PPI)

The subject mouse was placed in an animal holder and allowed to acclimate for 5 min without any stimulus, except the background white noise. Subsequently, the mouse underwent three blocks of different startle stimuli. Blocks 1 and 3 comprised ten trials of a 120 dB startle stimulus without a pre-pulse. The inter-trial intervals were randomly varied between 10 and 15 s. In Block 2, the PPI testing phase, a total of 56 trials were conducted. This included 8 trials of the startle stimulus alone, 32 trials of a prepulse stimulus (67, 70, 73, or 76 dB) followed by the startle stimulus, 8 trials of the prepulse alone (two at each intensity), and 8 null trials without any stimulus, each lasting 200 ms. The prepulse stimulus lasted 20 ms and was followed by a fixed interval of 100 ms. All trials were presented in a pseudo-random order. The duration of the startle stimulus was 40 ms in all blocks, and the background noise was set at 62 dB. The SOF-825 Startle Reflex System (Med Associates Inc.) recorded the amplitudes of the startle response in each trial. The apparatus was cleaned with 75% ethanol between each animal.

PPI % was calculated as (1–Mean response amplitude after prepulse and startle stimuli/Mean response amplitude after startle stimuli alone) × 100. The startle response was determined by the mean of peak amplitude in Block 1.

Stereotaxic injection

$Grin2a^{fl/fl}$ mice were anesthetized with isoflurane and secured on the stereotaxic apparatus (RWD Life Science Inc., 69100). Continuous isoflurane administration through an anaesthesia machine (Smiths Medical PM, Inc., V7300220) was maintained, while the mice were kept warm at 34 °C using a heating pad. Small holes were drilled in the skull to enable bilateral injection of viruses (Shanghai Taitool Bioscience Co.Ltd., AAV2/9-hSyn-Cre-EGFP, S0230-9, AAV2/9-hSyn-EGFP, S0237-9; 200 nl/injection site) into the medial prefrontal cortex (M/L, ± 0.4 mm; A/P, 1.8 mm; D/V, –1.7 mm from bregma) or hippocampus (M/L, ± 1.5 mm; A/P, –2 mm; D/V, –1.5 mm from bregma). Mice were allowed to recover for at least 3 weeks before performing behavioural tests.

Real-time quantitative PCR

Total RNA from the mPFC was purified using the TRIzol Reagent (Invitrogen, 15596026). qRT-PCR was conduct with QuantiTect RT-PCR Kits (Qiagen, 204443) and the QuantStudio™ 6 Flex Real-Time PCR System (Thermo Fisher Scientific, 4485691). The β-Actin gene served as an internal control (forward primer: 5′-GGC TGT ATT CCC CTC CAT CG-3′, reverse primer: 5′-CCA GTT GGT AAC AAT GCC ATG T-3′). The primers for other genes were purchased from Qiagen, Inc (QT01660057, QT00134302, QT00104272, QT00239295, QT00163527).

Immunostaining

Mice underwent deep anaesthesia using isoflurane and were subsequently intracardially with PBS (phosphate buffered saline) followed by 4% paraformaldehyde (PFA). Brain samples were fixed in 4% PFA at 4 °C overnight and then dehydrated in a PBS solution containing 30% sucrose at 4 °C until tissues sank. Brain slices, with a thickness of 40 μm (Leica CM3050S), were prepared and stored in cryoprotectant solution at 4 °C. Following three PBS washes, slices were blocked with 1% BSA for 1 h at room temperature. The primary antibodies (Rabbit-anti-GFP, 1:1000, Thermo Fisher Scientific, A11122; Rabbit-anti-NPY, 1:1000, Cell Signalling Technology, 11976S; Mouse-anti-GAD1, 1:1000, Millipore, MAB5406) were incubated at 4 °C overnight, followed by three PBS washes. Subsequently, slices were exposed to the secondary antibodies (Alexa Fluo 488, 1:1000, Invitrogen, A11034; Alexa Fluo 568, 1:1000, Invitrogen, A11031) at room temperature for 1 h. After three PBS washes, the slices were mounted for imaging using an Andor spinning disk confocal microscope. Image processing and analysis were conducted using ImageJ and Imaris software.

Fluorescence in situ hybridization

The GluN2A probe was cloned into the pGEM-T vector (Promega, A3600), transcribed in vitro, and labelled with digoxygenin (DIG)-UTP (Roche, 3359247910). The RNA probes were purified using mini–Quick Spin Columns (Roche, 11814427001) containing Sephadex G-50 matrix. For FISH, fresh-frozen brain sections underwent washing with DEPC-PBS, blocking of endogenous peroxidase with 2% H_2O_2 in DEPC-PBS, and sequential permeabilization with 0.2 M HCl and 0.3% Triton X-100 in DEPC-PBS. Sections were then treated with 0.25% Triethanolamine-Acetic anhydride to minimize nonspecific background. For the hybridization reaction, sections were pre-hybridized in the hybridization solution (50% formamide, 5 × saline-sodium citrate (SSC), 5 mM EDTA, 0.3 mg/ml yeast tRNA, 100 μg/ml heparin, 1 × Denhardt's solution, 0.1% Tween-20, and 0.1% CHAPS in DEPC-H_2O) for 1 h at 60 °C, followed by hybridization in the same solution containing 1 μg/ml GluN2A probe for 16–20 h in a 60 °C water bath. Sections were then washed twice in 2 × SSC buffer at 60 °C, once in 10 μg/ml RNase buffer at 37 °C to remove unbound RNA probe and three times in 0.2 × SSC buffer at 60 °C. Subsequently, sections were blocked with 10% goat serum in PBST for 15 min at room temperature and incubated with Anti-DIG-POD (Roche, 11207733910) at 4 °C overnight with a 1:500 dilution. Visualization of DIG-labelled probes was achieved by incubating sections with Cy3-tyramide (PerkinElmer, NEL704A001KT). In some experiments IHC staining was performed after

FISH. All images were taken 24 h after the mounting procedure.

Slice preparation

Mice aged 7–8 weeks underwent anaesthesia using isoflurane and were subsequently euthanized via cervical dislocation. The entire brain was swiftly dissected and placed in a cool, oxygenated cutting buffer comprising (in mM): 110 Choline Cl, 2.5 KCl, 1.25 NaH_2PO_4, 25 $NaHCO_3$, 7 $MgSO_4$, 25 D-glucose, 3.1 Na Pyruvate, 11.6 Na Ascorbate, 0.5 $CaCl_2$ at pH 7.25 (300 mOsm).[35] Coronal slices containing the medial prefrontal cortex (mPFC), 200 μm in thickness, were cut using a vibratome (Leica VT1200S) and promptly transferred to artificial cerebrospinal fluid (ACSF) containing (in mM): 127 NaCl, 2.5 KCl, 12.5 NaH_2PO_4, 25 $NaHCO_3$, 25 D-glucose, 2.5 $CaCl_2$, 1.3 $MgCl_2$, and oxygenated with 95% O_2/5% CO_2 to maintain a pH of 7.25.[35] Slices were incubated at 34 °C for 30 min and then allowed to recover at room temperature for an additional 30 min before recordings were initiated, which were conducted at room temperature.

Electrophysiological recording

Electrophysiological recordings were conducted according to established procedures. Whole-cell recordings were acquired from pyramidal neurons in layer 5 of the mPFC. Recording electrodes (TW150F-4, World Precision Instruments) filled with an internal solution containing (in mM): 115 caesium methanesulfonate, 20 CsCl, 10 HEPES, 2.5 $MgCl_2$, 4 Na_2ATP, 0.4 Na_3GTP, 10 Na phosphocreatine, and 0.6 EGTA (pH 7.25) were utilized, yielding a resistance of 4–6 MΩ. EPSCs and IPSCs were recorded in voltage-clamp mode using a multiclamp 700 B amplifier (Molecular Devices). Signals were filtered at 2 kHz and digitized at 20 kHz with an Axon Digidata 1440A analogue-to-digital board (Molecular Devices, CA). Miniature excitatory post-synaptic currents (mEPSCs) were recorded at a holding potential of −70 mV with 1 μM tetrodotoxin (TTX, MedChem express, HY-12526A) and 100 μM picrotoxin (PTX, Sigma, P1675). Miniature inhibitory post-synaptic currents (mIPSCs) were recorded at a holding potential of 0 mV with 1 μM TTX in ACSF. Spontaneous excitatory post-synaptic currents (sEPSCs) were recorded at −70 mV holding potential in the presence of 100 μM PTX, and spontaneous inhibitory post-synaptic currents (sIPSCs) were recorded at 0 mV holding potential. Data analysis was performed using MiniAnalysis software (Synaptosoft).

EEG/EMG

Mice aged 3-6 months were anesthetized with isoflurane (~3.5% at 700 mL/min) and administered a subcutaneous injection of 4 mg/kg of Carprofen (Henry Schein, Dublin, OH, USA). A prefabricated 6-pin, 3-channel headmount (2 EEG channels, one EMG; model #8201 Pinnacle Technologies, Lawrence KS, USA) was affixed to the skull with two 0.10″ screws anterior (#8209, Pinnacle Technologies) and two 0.12” screws posterior (#8212, Pinnacle Technologies) implanted at the following stereotactic coordinates relative to bregma (lateral, anterior in mm): reference electrode: −1.2, −2.5; animal ground electrode: −1.2, 3; EEG channel one electrode: 1.2, −2.5; EEG channel two electrode: 1.2, 3. Silver epoxy (#8226, ResinLab, Germantown WI, USA) was applied to the screws to ensure electrical conduction, and the assembly was secured to the skull with VetBond (#1469SB 3M, Saint Paul MI, USA) and dental acrylic (#1230, Lang Dental Manufacturing, Wheeling IL, USA). EMG electrodes were inserted into small pockets in the nuchal muscle.

Synchronized video, EEG, and EMG recordings

During the mid–light cycle, mice were subjected to 2.5 h of recording in four cylindrical acrylic arenas, each with a diameter of 25.4 cm, and containing bedding. Recordings utilized 4-channel video/tethered-EEG systems from Pinnacle Technologies. The EEG and EMG data were sampled at a resolution of 16 bits and a frequency of 500 Hz. EEG data were band-pass filtered between 0.5 and 125 Hz, while EMG data were filtered between 10 and 125 Hz. Grayscale videos with a resolution of 320 × 240 pixels were captured at a rate of 10 frames per second.

Video EEG/EMG analysis

For all analyses and plots, data collected over the frontal cortex (EEG channel two) were employed. The EEG/EMG data were exported to European Data Format (.edf) files for subsequent analysis in Matlab 2016b (Mathworks, Natick, MA, USA). Spectrograms were computed using the multitaper method with three tapers, 1-s windows, 0.1-s steps, and 2 Hz bandwidths, employing the Chronux toolbox (http://chronux.org).[36] The spectrograms were then averaged into 5-s epochs for sleep state classification using a 3-step semi-automated hierarchical algorithm based on the EMG and EEG channel 2 signals.[37] Briefly, the step 1 threshold was manually chosen to best separate the EMG_{RMS} signal (above threshold = Active Wake, below threshold = next step). The step 2 threshold separated $(\delta*\alpha)/(\beta*\gamma)$ (above = NREM, below = next step), and the step 3 threshold separated $(\theta^2)/(\delta*\alpha)$ (above = REM, below = Quiet Wake). Active Wake and NREM comprised 96% of the total epochs. The frequency bands for sleep scoring were defined as follows: δ = 0.5–6 Hz, θ = 6–10 Hz, α = 10.5–15 Hz, β = 22–30 Hz, and γ = 35 to 56 and 64–100 Hz, avoiding potential 60 Hz noise. EEG power across frequencies was normalized to total power from 0.5 to 100 Hz for plotting. To detect EEG spikes, line length features[38] were first extracted from the raw data as:

$$ll = f * |x(n) - x(n-1)|$$

Where ll is the line length trace, f is a 15 ms averaging window, * is a convolution operation, and $x(n)$ is the raw EEG amplitude at sample n.

EEG spikes were then identified in the line length trace as wherever:

$$ll(n) > 10 \times std(ll)$$

using the *findpeaks* function in Matlab with a 200 ms minimum inter-peak distance.

Western blotting

Cortex lysates were acquired using RIPA buffer (Solarbio, R0010) and heated at 95 °C for 10 min, followed by centrifugation at 12,000 × *g* for 10 min. We loaded 10 μg of protein onto an 8% Tris-glycine SDS-PAGE gel for protein separation, subsequently transferring them to nitrocellulose membranes. To minimize non-specific binding, the membranes underwent blocking in 5% (w/v) non-fat milk for 1 h at room temperature, followed by three washes with tris-buffered saline containing 0.1% Tween 20 detergent (TBST) for 5 min each. Primary antibodies (GluN2A, 1:1000, Novusbio, NB300-105; β-Actin, 1:1000, Cell Signalling Technology, 3700S) were incubated at 4 °C overnight. After three additional washes with TBST, the membranes were exposed to anti-rabbit/mouse HRP-conjugated secondary antibodies (33101ES60, 1:10000, Yeasen) for 1 h at room temperature and visualized using an ECL Kit (36222ES60, Yeasen) and a chemiluminescence imaging system (FUSION FX, Vilber). The β-Actin signal served as a loading control, facilitating the normalization of differences resulting from variations in the amount loaded.

Ethics statement

All animal procedures received approval from the Institutional Animal Care and Use Committee of Animal Facility at the National Facility for Protein Science in Shanghai (NFPS), Shanghai Advanced Research Institute, Chinese Academy of Sciences, China, and adhered to the National Institutes of Health's Guide for the Care and Use of Laboratory Animals. The reference number of the approvals of the animal study is IACUC 202003080007.

Statistical analyses

All statistical tests were two-tailed, and significance was set at $p < 0.05$. Normality was assessed using the Shapiro–Wilk test, and equal variances were assessed using the F test and Brown–Forsythe test. When normality and equal variance between sample groups were met, we employed t-test (two-tailed), one-way ANOVA (followed by Tukey's multiple comparisons test), repeated measures two-way ANOVA (followed by Tukey's or Bonferroni's comparisons test), and two-way ANOVA (followed by Fisher's LSD). In cases of failed normality or equal variance, Kruskal–Wallis one-way ANOVA (followed by Dunn's multiple comparisons test), Mann–Whitney U test and Unpaired t-test with Welch's correction (two-tailed). The Kolmogorov–Smirnov test was applied to compare cumulative distributions. All statistical analyses were performed using GraphPad Prism v8. Data are presented as the mean ± SEM $*p < 0.05$, $**p < 0.01$, $***p < 0.001$, $****p < 0.0001$, n.s., not significant. Supplementary Information Table S1 provides details on sample sizes, specific statistical tests used, and main effects of statistical analyses for each experiment.

Role of funders

Funders played no role in the study design, the collection, analyses and interpretation of data, the preparation of the manuscript, or decision to publish.

Results

Germline GluN2A KO mice exhibits several aspects of schizophrenia-related phenotypes

To assess whether the loss of GluN2A leads to schizophrenia-related phenotypes in mice, we conducted a series of tests comparing adult germline GluN2A$^{-/-}$ mice with their wildtype littermates (GluN2A$^{+/+}$). The absence of GluN2A protein in GluN2A$^{-/-}$ mice and the approximately 50% reduction of GluN2A protein in GluN2A$^{+/-}$ mice were confirmed through western blotting (Supplementary Fig. S2a and b).

In the open field test (OFT), hyperactivity is associated with positive symptoms of schizophrenia.[39,40] Adult GluN2A$^{-/-}$ mice travelled approximately 110% farther than their WT littermates, indicating of increased locomotor activity (Fig. 1a and b), consistent with a previous study.[41] Negative symptom-related behavioural abnormalities were then assessed.[39,40] In the nest building test (NBT), adult GluN2A$^{-/-}$ mice left significantly more unused nesting materials compared to WT littermates (Fig. 1c and d). In the three-chamber social test (TCST), GluN2A$^{-/-}$ mice spent a comparable amount of time to WT littermates in preference for the stranger mouse (S1) over an empty chamber, suggesting intact "sociability" (Fig. 1e and f). However, unlike WT mice, which tended to spend more time in the chamber with a new stranger mouse (S2) compared to S1, GluN2A$^{-/-}$ mice spent similar amounts of time with S2 and S1, indicating impaired "social novelty preference" (Fig. 1g and h). Overall, the NBT and TCST results suggest that GluN2A knockout can reflect negative symptoms of schizophrenia in mice.

To evaluate cognitive function and spatial working memory, we measured the spontaneous alternation of GluN2A$^{-/-}$ mice in the Y maze test and found that the normalized spontaneous alternation was significantly lower compared to their WT littermates (Fig. 1i), indicating spatial working memory deficits in GluN2A KO mice. GluN2A$^{-/-}$ mice made approximately 55% more entries than WT littermates, further suggesting hyperactivity (Fig. 1j).

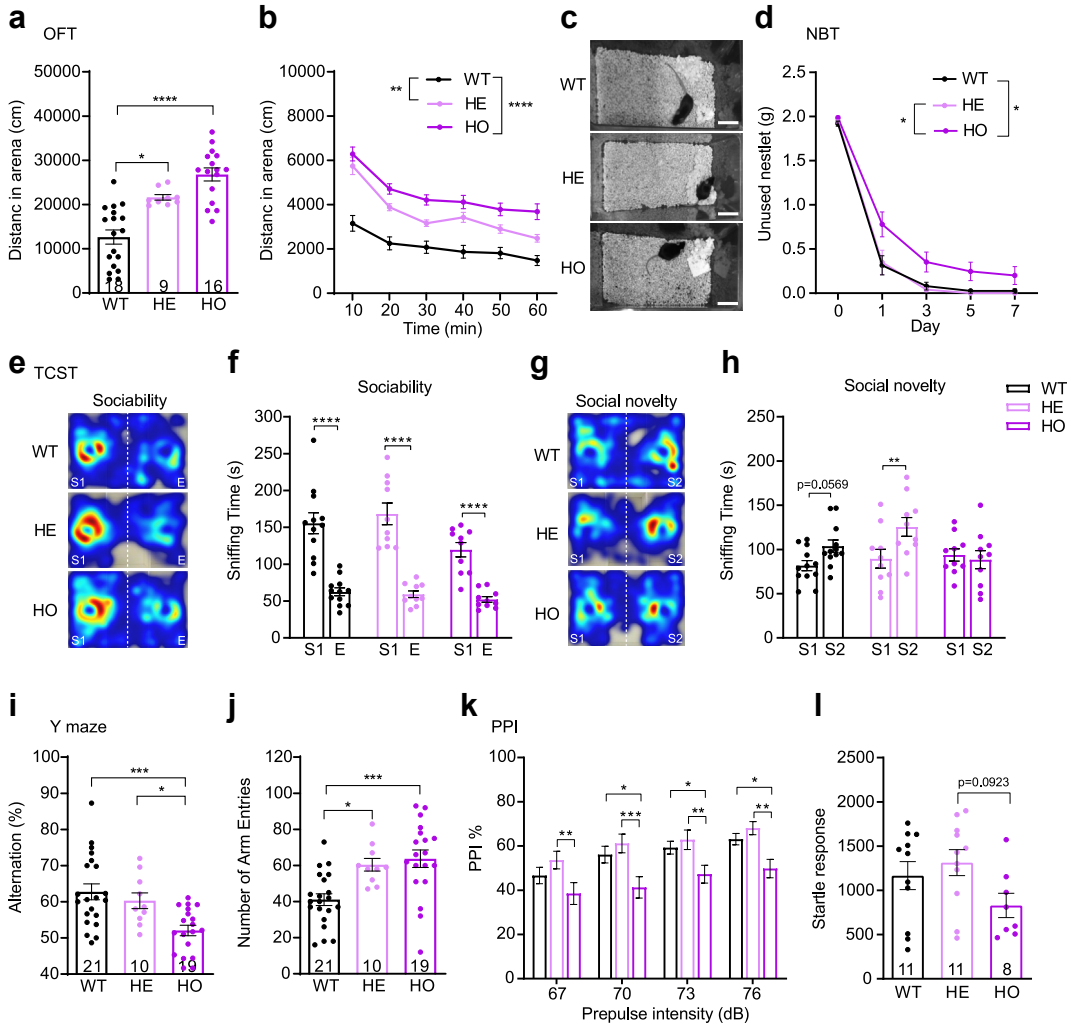

Fig. 1: **Germline GluN2A KO mice exhibited many aspects of schizophrenia-related behaviours, including positive, negative, cognitive and PPI deficits.** (a and b) The total distance (a) and travel distance per 10 min (b) in the open field test. WT, GluN2A$^{+/+}$ mice; HE, GluN2A$^{+/-}$ mice; HO, GluN2A$^{-/-}$ mice (WT *n* = 18, HE *n* = 9, HO *n* = 16). (c and d) The representative pictures (c) and quantitation (d) of unused nestlet materials in nest building test (WT *n* = 20, HE *n* = 12, HO *n* = 19). Scale bar, 3 cm. (e and f) Heatmap (e) and sniffing time (f) of sociability in three chamber social test. E, empty chamber; S1, stranger 1 (WT *n* = 12, HE *n* = 10, HO *n* = 10). (g and h) Heatmap (g) and sniffing time (h) of social novelty in three chamber social test. S1, stranger 1; S2, stranger 2 (WT *n* = 12, HE *n* = 10, HO *n* = 10). (i and j) The alternation percentage (i) and number of arm entries (j) in Y maze spontaneous alternation test (WT *n* = 21, HE *n* = 10, HO *n* = 19). (k and l) The percentage of PPI (k) and startle response (l) in prepulse inhibition test (WT *n* = 11, HE *n* = 11, HO *n* = 8). Error bars show S.E.M. **p* < 0.05, ***p* < 0.01, ****p* < 0.001, *****p* < 0.0001. See Supplementary Table S1 for statistical analysis.

Prepulse Inhibition (PPI) is the normal suppression of the startle reflex when a barely detectable prepulse stimulus is presented shortly before the startling stimulus. Startle habituation is the decrease in response that occurs when the same stimulus is presented repeatedly. These factors have been proposed as neurophysiological measures of sensorimotor gating and have been considered as trait-linked markers for information-processing deficits, often observed as impaired in schizophrenia[39,40,42] GluN2A$^{-/-}$ mice exhibited a significantly smaller PPI ratio (PPI%) than WT littermates when prepulse stimuli of 70, 73, or 76 dB were presented before the startle response (Fig. 1k). We also observed a trend towards a smaller startle response in GluN2A$^{-/-}$ mice in this test (Fig. 1l). These findings implicated that GluN2A depletion disrupts sensorimotor gating, aligning with the symptoms observed in patients.

Heterozygous GluN2A$^{+/-}$ mice, representing a genetic model with a partial loss of GluN2A function, exhibited increased distance travelled in the OFT compared to WT mice, though to a lesser extent than GluN2A$^{-/-}$ mice (Fig. 1a and b). In the remaining

behavioural tests, GluN2A$^{+/-}$ mice did not manifest significant differences from their WT littermates. These findings align with previous genetic studies indicating an elevated risk of schizophrenia associated with heterozygous loss-of-function mutations in GluN2A.[15,16,43] The more pronounced abnormalities observed in GluN2A null mice may reflect more readily detectable conditions in these rodent behavioural models.

Depletion of GluN2A in late postnatal development resulted in various schizophrenia-related phenotypes in mice, while its adult deletion only led to negative-related symptoms

Prior studies demonstrated that early postnatal ablation of GluN1 in forebrain interneurons fully recapitulated schizophrenia-related phenotypes in mice, whereas depletion in adult brains did not.[40,44] We explored whether adult depletion of GluN2A would induce schizophrenia-related phenotypes and whether this outcome depended on the cell type in which GluN2A was ablated.

To address these questions, we generated UBC-CreERT2$^{+/-}$::Grin2a$^{fl/fl}$ mice (Supplementary Fig. S2c and d) enabling the knockout of GluN2A in adult mice (12 weeks old and above) through tamoxifen (TAM) treatment (Fig. 2a and b). Intriguingly, the induction of GluN2A conditional knockout (cKO) in adult mice did not result in schizophrenia-related phenotypes in mice compared to control mice (UBC-CreERT2$^{-/-}$::Grin2a$^{fl/fl}$) in several behavioural tests associated with schizophrenia, including OFT (Fig. 2c and d), Y maze spontaneous alternation test (Fig. 2j and k), and PPI test (Fig. 2l and m). However, adult GluN2A cKO mice did exhibit deficits in nest building (Fig. 2e) and social novelty behaviour (Fig. 2f–i). These findings support the notion that the loss of GluN2A in adult brains is sufficient to cause negative-related symptoms, while positive-related and cognitive symptoms result from the loss of GluN2A during developmental stages.

Furthermore, we analysed the time window for the induction of GluN2A depletion-induced schizophrenia-related phenotypes (Fig. 3a). Remarkably, late postnatal depletion of GluN2A (7–8 weeks old; Supplementary Fig. S2e and f) led to the complete recapitulation of behavioural abnormalities observed in GluN2A$^{-/-}$ mice, including hyperlocomotion (~32% higher total travel distance than WT controls; Fig. 3b and c), nest building defects (Fig. 3d), impaired Y maze performance (~12% reduction in normalized alternation; Fig. 3e and f), and reduced PPI ratios (~37% decrease with 70, 73, or 76 dB prepulse stimulus; Fig. 3g and h). These results indicate that the loss of GluN2A during late postnatal development remains sufficient to mimic many aspects of schizophrenia-related phenotypes in mice.

Loss of GluN2A in excitatory or inhibitory neurons recapitulates overlapping but different schizophrenia-related phenotypes in mice

The involvement of NMDARs in both excitatory and inhibitory neurons have been established in schizophrenia.[44–46] To explore the contributions of GluN2A in different neuronal subtypes, we generated and analysed mice with excitatory and inhibitory neuron-specific GluN2A KO.

For the targeted deletion of GluN2A in excitatory neurons, we crossed Grin2a$^{fl/fl}$ mice with NEX-Cre mice, expressing Cre recombinase exclusively in cortical and hippocampal excitatory neurons.[47] Western blot analyses confirmed an 80% reduction in GluN2A proteins in the cortex of NEX-Cre GluN2A cKO mice (Supplementary Fig. S2j and k). Fluorescence in situ hybridization (FISH) revealed a consistent anatomical pattern of selective loss in excitatory neurons (Supplementary Fig. S2l and m). Similar to GluN2A$^{-/-}$ mice, NEX-Cre GluN2A cKO mice exhibited significant increases in distance travelled in the OFT (Fig. 4a and b), left more unused nestlets in the NBT (Fig. 4c), failed to differentiate between a new stranger mouse and a familiar mouse in the TCST (Fig. 4d–g), and displayed impaired PPI% compared to NEX-Cre wild-type mice (Fig. 4j and k). However, they did not manifest any defects in the Y maze tests (Fig. 4h and i), in contrast to the GluN2A$^{-/-}$ mice.

For the specific deletion of GluN2A in inhibitory neurons, we crossed Grin2a$^{fl/fl}$ mice with vGAT-Cre mice, expressing Cre recombinase solely in inhibitory neurons.[48] Approximately ~30% of GluN2A was depleted in the cortex of inhibitory neuron-specific GluN2A cKO mice (vGAT-Cre GluN2A cKO; Supplementary Fig. S2g and h). FISH analysis confirmed selective depletion in GAD1-stained inhibitory interneurons (Supplementary Fig. S2i). Intriguingly, the inhibitory neuron-specific GluN2A KO mice exhibited deficits in the NBT (Fig. 5c), TCST (Fig. 5d–g), and PPI (Fig. 5j and k), but not in the OFT (Fig. 5a and b) and Y maze tests (Fig. 5h and i).

These findings indicate that the loss of GluN2A in cortical and hippocampal excitatory neurons alone is sufficient to induce schizophrenia-related behavioural phenotypes encompassing positive and negative symptoms, as well as sensorimotor gating deficits. In contrast, the loss of GluN2A in inhibitory interneurons alone is sufficient to cause deficits specifically in negative-related phenotypes and sensorimotor gating. Notably, GluN2A loss in either cell type alone did not lead to cognitive phenotypes in the Y maze.

Depletion of GluN2A in hippocampus or mPFC before adulthood results in overlapping yet distinct behavioural defects resembling schizophrenia-related phenotypes in mice

Given prior evidence illustrating abnormalities induced by the loss of GluN2A from the cortex and hippocampus (Fig. 4) and considering the relevance of these brain

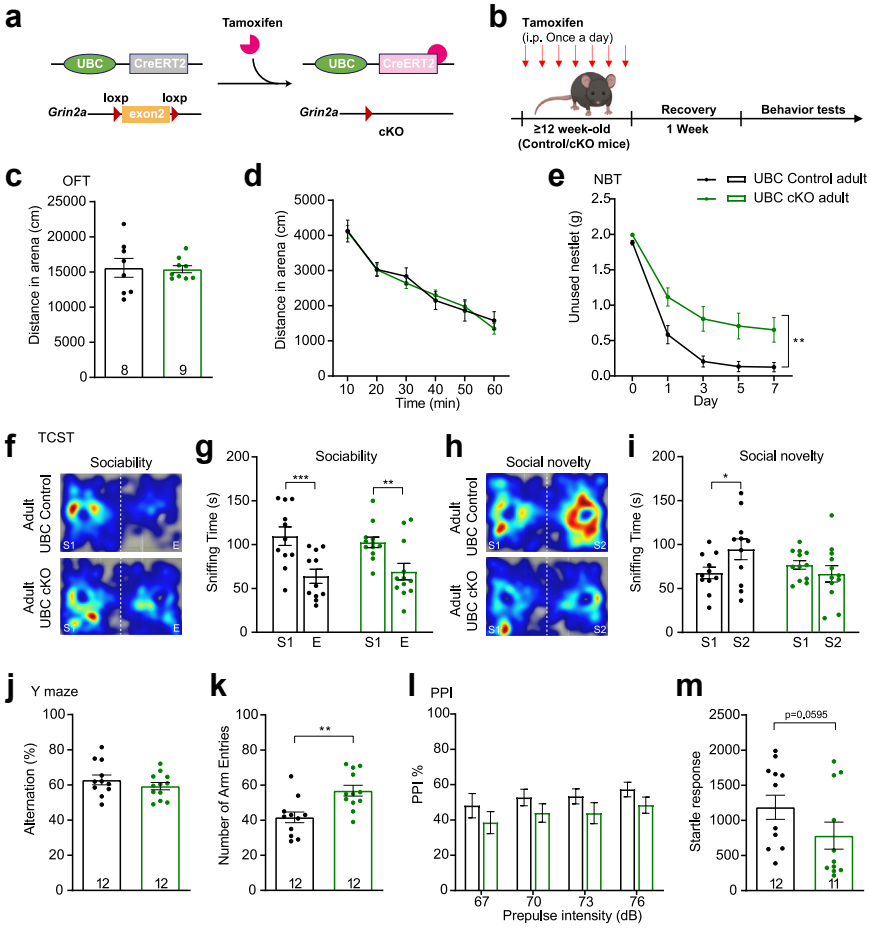

***Fig. 2:* Knockout of GluN2A in adult mice induced only negative symptom-related abnormalities.** (a and b) Schematic diagrams of tamoxifen (TAM) inducible system (a) and the experimental schedule for inducible KO of GluN2A in adults (b). UBC-CreERT$^{-/-}$::Grin2a$^{fl/fl}$ mice (UBC Control adult) and UBC-CreERT$^{+/-}$::Grin2a$^{fl/fl}$ mice (UBC cKO adult) at greater than 12 weeks were injected intraperitoneally with TAM once a day for 7 days. Behavioural evaluations were performed after a week of recovery following injections. (c and d) The total distance (c) and travel distance per 10 min (d) in open field test (UBC Control adult *n* = 8, UBC cKO adult *n* = 9). (e) The weight of unused nestlet materials in nest building test (UBC Control adult *n* = 12, UBC cKO adult *n* = 12). (f and g) Heatmap (f) and sniffing time (g) of sociability in three chamber social test. E, empty chamber; S1, stranger 1 (UBC Control adult *n* = 11, UBC cKO adult *n* = 12). (h and i) Heatmap (h) and sniffing time (i) of social novelty in three chamber social test. S1, stranger 1; S2, stranger 2 (UBC Control adult *n* = 11, UBC cKO adult *n* = 12). (j and k) The alternation percentage (j) and number of arm entries (k) in Y maze spontaneous alternation test (UBC Control adult *n* = 12, UBC cKO adult *n* = 12). (l and m) The percentage of PPI (l) and startle response (m) in prepulse inhibition test (UBC Control adult *n* = 12, UBC cKO adult *n* = 11). Error bars show S.E.M. **p* < 0.05, ***p* < 0.01, ****p* < 0.001. See Supplementary Table S1 for statistical analysis.

structures in psychiatric disorders,[16] we directed our focus toward understanding the role of GluN2A specifically in the hippocampus and mPFC.

To establish hippocampus-specific GluN2A knockout (hippo-cKO), we employed Adeno-associated virus (AAV) to express Cre recombinase and genetically remove GluN2A in the hippocampus of Grin2a$^{fl/fl}$ mice (Supplementary Fig. S3a and b). In the OFT, hippo-cKO mice travelled approximately 26% longer distances compared to control mice expressing enhanced green fluorescent protein (EGFP) in their hippocampus (Supplementary Fig. S3c and d). Additionally, the hippo-cKO mice exhibited impaired PPI% (Supplementary Fig. S3h and i). However, no deficits were observed in the NBT and Y maze tests (Supplementary Fig. S3e–g).

As for the mPFC-specific GluN2A knockout (mPFC-cKO) mice (Fig. 6a and b), they travelled approximately 64% longer distances in the OFT compared to mice expressing EGFP (Fig. 6c and d). The mPFC-cKO mice displayed defects in the NBT, leaving significantly more nesting materials than control mice (Fig. 6e). However, no deficits were observed in the TCST, Y maze tests, and PPI tests (Fig. 6f–m, respectively). These findings suggest that the knockout of GluN2A in the hippocampus

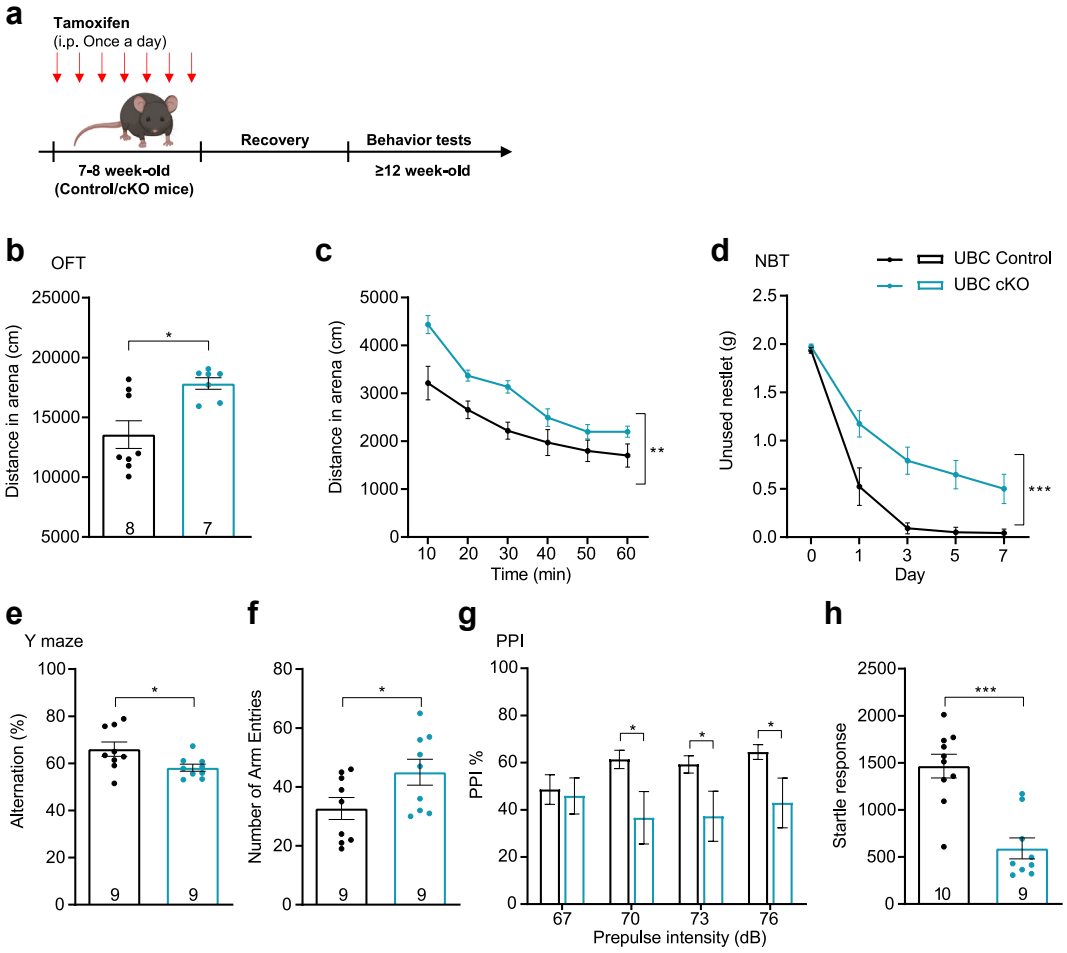

***Fig. 3*: GluN2A removal during late postnatal development led to many aspects of schizophrenia-related behavioural abnormalities in mice.** (a) Experimental schedule for inducible KO of GluN2A at 7–8 weeks. UBC-CreERT$^{-/-}$::Grin2a$^{fl/fl}$ mice (UBC Control) and UBC-CreERT$^{+/-}$::Grin2a$^{fl/fl}$ mice (UBC cKO) at 7–8 weeks were injected intraperitoneally with TAM once a day for 7 days. Behavioural tests were performed after the mice were 12 weeks old. (b and c) The total distance (b) and travel distance per 10 min (c) in open field test (UBC Control n = 8, UBC cKO n = 7). (d) The weight of unused nestlet materials in nest building test (UBC Control n = 10, UBC cKO n = 9). (e and f) The alternation percentage (e) and number of arm entries (f) in Y maze spontaneous alternation test (UBC Control n = 9, UBC cKO n = 9). (g and h) The percentage of PPI (g) and startle response (h) in prepulse inhibition test (UBC Control n = 10, UBC cKO n = 9). Error bars show S.E.M. *p < 0.05, **p < 0.01, ***p < 0.001. See Supplementary Table S1 for statistical analysis.

or mPFC during this late developmental stage is sufficient to induce behavioural defects related to schizophrenia in adulthood.

In contrast, when GluN2A was knocked out in the hippocampus or mPFC of adult mice (after 12 weeks old), deficits in the OFT, Y maze tests, and PPI tests were not observed (Supplementary Fig. S4). This underscores the critical role of the timing of GluN2A dysfunction during development in inducing schizophrenia-related behavioural abnormalities.

Loss of GluN2A induces alterations related to interneurons

To explore the molecular and synaptic mechanisms associated with GluN2A depletion, we focused on GluN2A$^{-/-}$ mice, displaying a broad range of phenotypes. Given the connection between inhibitory neuron dysfunction (GABAergic interneurons) in the mPFC and schizophrenia,[45] we examined the impacts of GluN2A deletion on the mRNA expression of five interneuron-related genes using RT-qPCR (Fig. 7g). Among them, neuropeptide Y (NPY) somatostatin (SST), and cortistatin (CORT) showed a significant increase in expression in GluN2A$^{-/-}$ mice (Fig. 7g).

Notably, NPY alterations have been associated with schizophrenia,[49,50] and NPY can promote dopamine release by activating sigma (σ) receptors.[51] Immunofluorescence staining revealed a significant ~89% increase in the density of NPY-positive cells in mPFC of

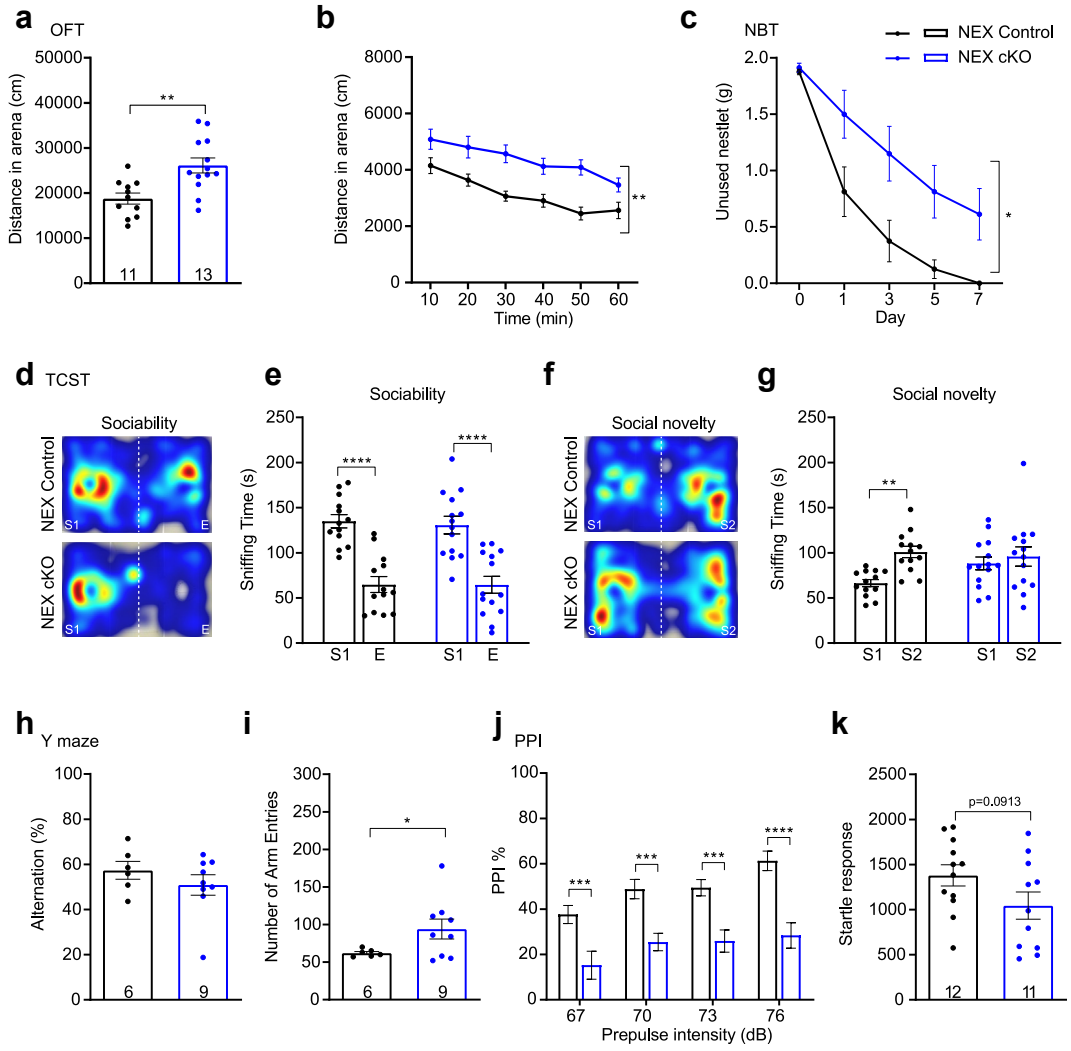

***Fig. 4:* Loss of GluN2A in excitatory neurons induced positive, negative symptom-related abnormalities and PPI deficits.** (a and b) The total distance (a) and travel distance per 10 min (b) in open field test. NEX Control, NEX-Cre$^{-/-}$::Grin2a$^{fl/fl}$ mice; NEX cKO, NEX-Cre$^{+/-}$::Grin2a$^{fl/fl}$ mice (NEX Control n = 11, NEX cKO n = 13). (c) The weight of unused nestlet materials in nest building test (NEX Control n = 8, NEX cKO n = 8). (d and e) Heatmap (d) and sniffing time (e) of sociability in three chamber social test. E, empty chamber; S1, stranger 1 (NEX Control n = 13, NEX cKO n = 14). (f and g) Heatmap (f) and sniffing time (g) of social novelty in three chamber social test. S1, stranger 1; S2, stranger 2 (NEX Control n = 13, NEX cKO n = 14). (h and i) The alternation percentage (h) and number of arm entries (i) in Y maze spontaneous alternation test (NEX Control n = 6, NEX cKO n = 9). (j and k) The percentage of PPI (j) and startle response (k) in prepulse inhibition test (NEX Control n = 12, NEX cKO n = 11). Error bars show S.E.M. *p < 0.05, **p < 0.01, ***p < 0.001, ****p < 0.0001. See Supplementary Table S1 for statistical analysis.

GluN2A$^{-/-}$ mice (Fig. 7h). However, this increase was not statistically significant in adult-induced GluN2A knockout mice (Fig. 7i), indicating that the regulation of NPY by GluN2A is developmentally stage-dependent. Interestingly, we detected a significant ~34% increase in the density of NPY-positive cells in mPFC of NEX-Cre GluN2A conditional knockout mice (Fig. 7j), suggesting that the loss of GluN2A in excitatory neurons alone is sufficient to regulate the expression of NPY, likely through non-cell autonomous mechanisms.

Loss of GluN2A in mPFC through germline deletion or during late postnatal development results in synaptic deficits

To evaluate the impact of GluN2A deletion on synaptic transmission in the mPFC, we conducted whole-cell patch-clamp recordings on pyramidal neurons in layer 5 of the mPFC using acute brain slices from GluN2A$^{-/-}$ mice. Surprisingly, the frequency and amplitude of miniature inhibitory post-synaptic currents (mIPSCs; Supplementary Fig. S5a and b) and spontaneous inhibitory post-synaptic currents (sIPSCs; Supplementary

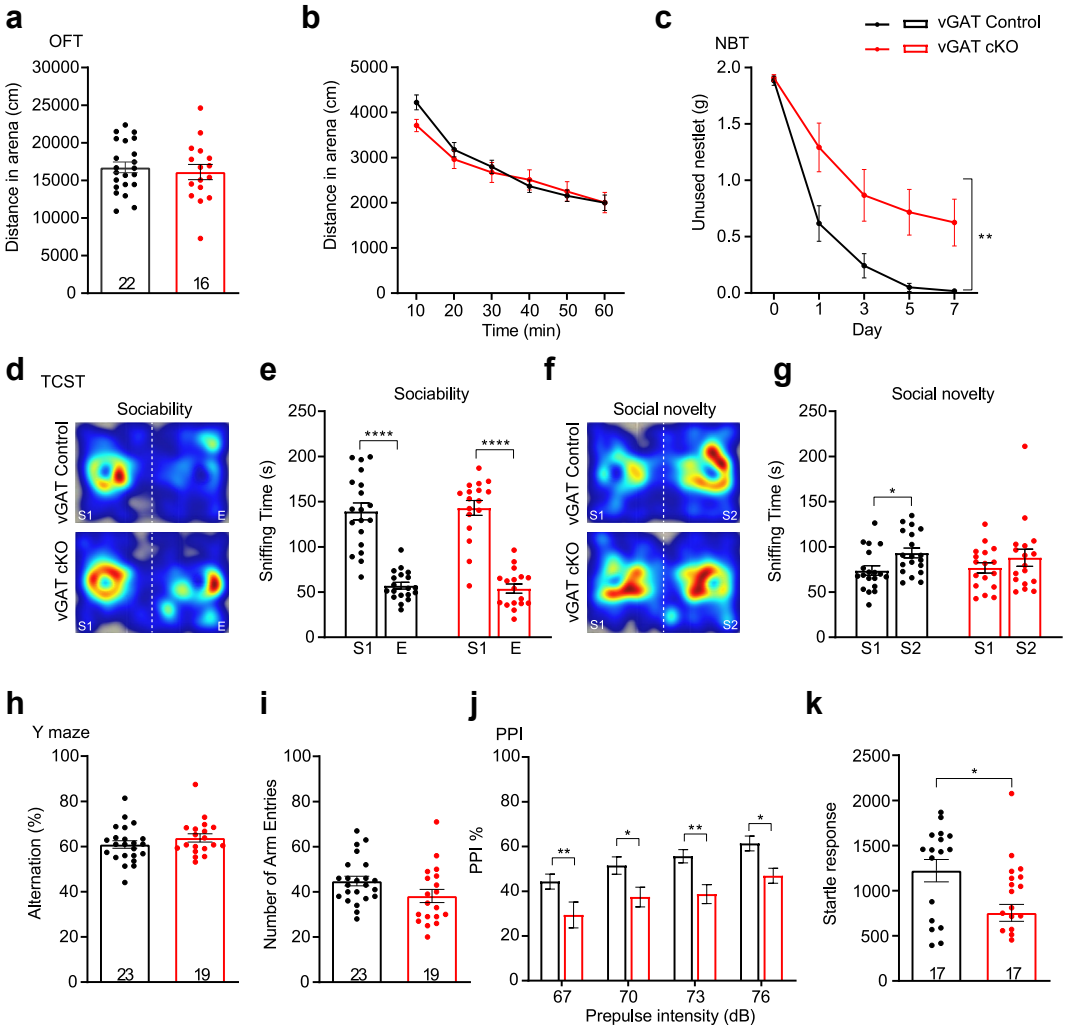

***Fig. 5:* Loss of GluN2A in inhibitory neurons induced only negative symptom-related abnormalities and PPI deficits.** (a and b) The total distance (a) and travel distance per 10 min (b) in open field test. vGAT Control, vGAT-Cre$^{-/-}$::Grin2a$^{fl/fl}$ mice; vGAT cKO, vGAT-Cre$^{+/-}$::Grin2a$^{fl/fl}$ mice (vGAT Control n = 22, vGAT cKO n = 16). (c) The weight of unused nestlet materials in nest building test (vGAT Control n = 12, vGAT cKO n = 12). (d and e) Heatmap (d) and sniffing time (e) of sociability in three chamber social test. E, empty chamber; S1, stranger 1 (vGAT Control n = 19, vGAT cKO n = 17). (f and g) Heatmap (f) and sniffing time (g) of social novelty in three chamber social test. S1, stranger 1; S2, stranger 2 (vGAT Control n = 19, vGAT cKO n = 17). (h and i) The alternation percentage (h) and number of arm entries (i) in Y maze spontaneous alternation test (vGAT Control n = 23, vGAT cKO n = 19). (j and k) The percentage of PPI (j) and startle response (k) in prepulse inhibition test (vGAT Control n = 17, vGAT cKO n = 17). Error bars show S.E.M. *p < 0.05, **p < 0.01, ****p < 0.0001. See Supplementary Table S1 for statistical analysis.

Fig. S5c and d) were not significantly altered in GluN2A knockout mice. However, the frequency of miniature excitatory post-synaptic currents (mEPSCs; Fig. 7a and b) and spontaneous excitatory post-synaptic currents (sEPSCs; Fig. 7c and d) showed a significant increase of approximately 60% in the mPFC of GluN2A$^{-/-}$ mice compared to their WT controls. Notably, the amplitude of mEPSCs (Fig. 7a and b) and sEPSCs (Fig. 7c and d) remained unchanged.

We further assessed synaptic transmission in mPFC pyramidal neurons of GluN2A cKO mice (Supplementary Fig. S6). Depletion of GluN2A during late postnatal development led to a significantly increased frequency of mEPSCs and sEPSCs (Supplementary Fig. S6a–d), resembling the findings in GluN2A$^{-/-}$ mice. Moreover, the amplitude of sEPSCs but not mEPSCs was significantly increased in mice that experienced GluN2A loss during development (Supplementary Fig. S6a-d). These results suggest that the loss of GluN2A before adulthood induces abnormalities in excitatory synaptic transmission.

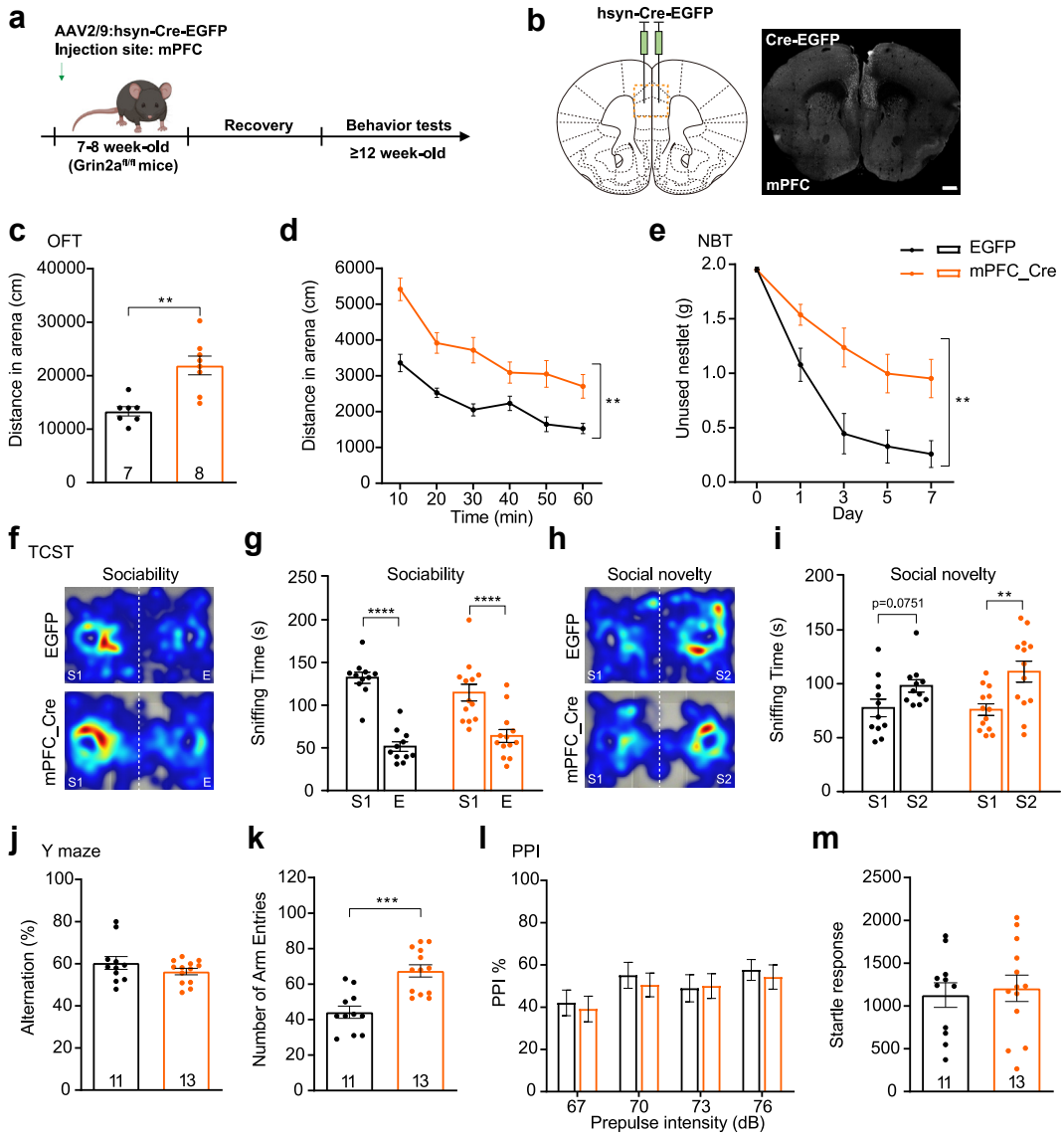

***Fig. 6:* Deletion of GluN2A in mPFC during late postnatal development induced positive and negative symptom-related abnormalities.** (a and b) Experimental schedule (a) for inducible KO of GluN2A in mPFC at 7–8 weeks and representative photomicrographs (b) of injection sites in the mPFC. Scale bar, 500 μm. (c and d) The total distance (c) and travel distance per 10 min (d) in open field test (EGFP n = 7, mPFC_Cre n = 8). (e) The weight of unused nestlet materials in nest building test (EGFP n = 11, mPFC_Cre n = 13). (f and g) Heatmap (f) and sniffing time (g) of sociability in three chamber social test. E, empty chamber; S1, stranger 1 (EGFP n = 11, mPFC_Cre n = 13). (h and i) Heatmap (h) and sniffing time (i) of social novelty in three chamber social test. S1, stranger 1; S2, stranger 2 (EGFP n = 11, mPFC_Cre n = 13). (j and k) The alternation percentage (j) and number of arm entries (k) in Y maze spontaneous alternation test (EGFP n = 11, mPFC_Cre n = 13). (l and m) The percentage of PPI (l) and startle response (m) in prepulse inhibition test (EGFP n = 11, mPFC_Cre n = 13). Error bars show S.E.M. $^{**}p < 0.01$, $^{***}p < 0.001$, $^{****}p < 0.0001$. See Supplementary Table S1 for statistical analysis.

In contrast, neither the frequency nor the amplitude of mEPSCs or sEPSCs were altered in mPFC pyramidal neurons from mice that lost GluN2A in adulthood (Supplementary Fig. S6e–h). These findings imply that the knockout of GluN2A in the mPFC during the developmental stage, rather than in adulthood, drives excitatory transmission rather than reducing inhibitory transmission, leading to physiological and behavioural changes related to schizophrenia.[46]

Loss of GluN2A induces alterations in brain network activity and oscillation

The observed changes in the density of NPY inhibitory interneurons and the frequency of EPSCs in pyramidal

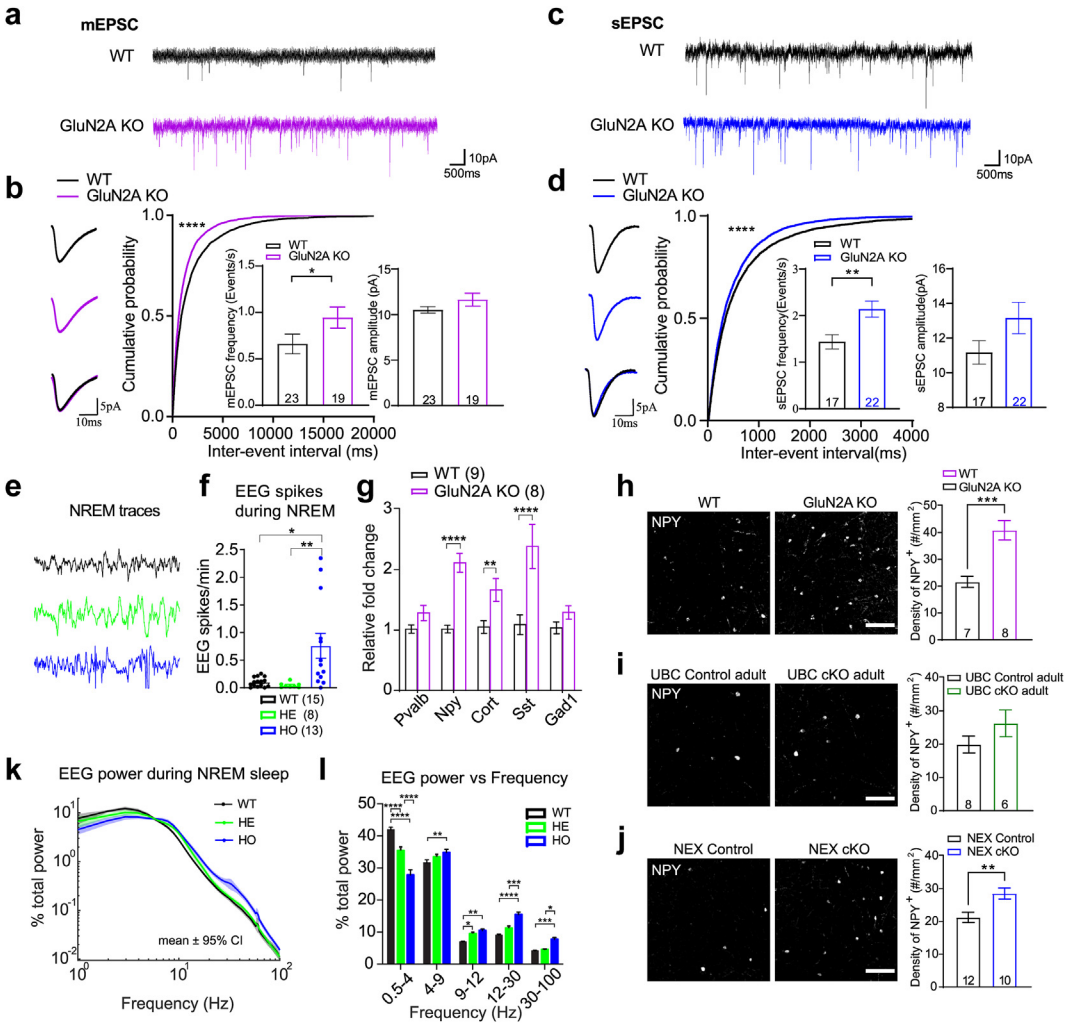

Fig. 7: **Knockout of GluN2A led to alterations in interneuron-related gene expression, excitatory synaptic transmission and brain network activity.** (a and b) The mEPSCs recordings from 7 to 8 weeks old WT or GluN2A KO mice. Representative traces (a), average individual events and cumulative plot of the interevent interval (b, left inset: mean frequency; right inset: mean amplitude) (WT n = 23, GluN2A KO n = 19). (c and d) The sEPSCs recordings from 7 to 8 weeks old WT or GluN2A KO mice. Representative traces (c), average individual events and cumulative plot of the interevent interval (d, left inset: mean frequency; right inset: mean amplitude) (WT n = 17, GluN2A KO n = 22). All the recordings were done in layer 5 of mPFC pyramidal neurons from WT (black) or GluN2A KO (purple or blue) mice. (e and f, k and l) EEG recordings during NREM sleep. Representative traces (e), spikes (f), and mean power spectra (k, quantified in l). WT, GluN2A$^{+/+}$ mice; HE, GluN2A$^{+/-}$ mice; HO, GluN2A$^{-/-}$ mice (WT n = 15, HE n = 8, HO n = 13). (g) Real-time qRT-PCR analysis of interneuron-related genes expression in cortex and hippocampus from WT and GluN2A KO mice (WT n = 9, GluN2A KO n = 8). (h–j) Representative images of NPY expression and quantitation of NPY density in mPFC of WT and GluN2A KO mice (h) (WT n = 7, GluN2A KO n = 8), adult CreERT$^{-/-}$::Grin2a$^{fl/fl}$ mice (UBC Control adult) and adult UBC-CreERT$^{+/-}$::Grin2a$^{fl/fl}$ mice (UBC cKO adult) in which inducible KO of GluN2A during adulthood (i) (UBC Control adult n = 8, UBC cKO adult n = 6), NEX-Cre WT mice and NEX-Cre GluN2A KO mice (j) (NEX Control n = 12, NEX cKO n = 10). Scale bar, 100 μm. Error bars show S.E.M. *p < 0.05, **p < 0.01, ***p < 0.001, ****p < 0.0001. See Supplementary Table S1 for statistical analysis.

neurons suggest that the deletion of GluN2A leads to complex alterations in cortical circuitry. Schizophrenia is characterized by elevated baseline gamma oscillations (30–100 Hz), a robust endophenotype.[46,52] To investigate network-level alterations, we examined the impact of GluN2A depletion on oscillation power using EEG recordings (Fig. 7e, f, k, l; Supplementary Fig. S7).

During NREM sleep, GluN2A$^{-/-}$ mice exhibited an elevated spike rate in the EEG, indicating synchronous network activity or epileptiform discharges (~8-fold increase) (Fig. 7e and f). This increase is consistent with the genetic association between GluN2A and syndromic epilepsy.[30,31] Additionally, they showed reduced power in the delta band (0.5–4 Hz) by 33%, while theta (4–9 Hz)

showed a 9% increase, alpha (9–12 Hz) showed a 52% increase, beta (12–30 Hz) showed a 72% increase, and gamma (30–100 Hz) showed a substantial 90% increase in power (Fig. 7k and l). GluN2A$^{+/-}$ mice generally displayed EEG powers between GluN2A$^{-/-}$ and wild-type mice, suggesting that oscillations were influenced by the level of GluN2A expression. These effects on oscillation power were most prominent during resting brain states, as no significant changes were observed during active wakefulness (Supplementary Fig. S7). Interestingly, the reduced oscillation power and increased spike rate, along with the cognitive impairments observed in GluN2A$^{-/-}$ mice, generally oppose the effects seen with pharmacological enhancement of GluN2A-containing NMDARs.[53]

Discussion

Schizophrenia presents a spectrum of clinically diverse manifestations,[4,54] posing a diagnostic challenge due to the potential disparity in symptoms between individuals. The reliance on diagnostic criteria may result in the categorization of individuals with distinct symptoms under the same disorder.[4,55] Understanding the underlying mechanisms of schizophrenia remains a significant hurdle in research, as the involvement of specific neurotransmitter systems, particularly the dopaminergic system, in only certain symptoms suggests diverse causative factors among patients.[9,10] Recent studies have emphasized that hypofunction of the glutamatergic system could instigate all schizophrenia-associated symptoms, indicating the potential role of NMDAR in the mechanistic understanding of these symptoms.

In the forebrain, GluN2A and GluN2B stand out as the principal subtypes of NMDARs, playing pivotal roles in schizophrenia.[22] Selective inhibitors or genetic depletion of GluN2B have demonstrated associations with schizophrenia-related phenotypes.[24–26] Conversely, large-scale human genetic studies have linked disruptive coding variants of GluN2A, not GluN1 or GluN2B, to an increased risk of schizophrenia,[15,16] underscoring GluN2A's involvement in the disorder's pathogenesis. Our findings unequivocally illustrate that genetic depletion of GluN2A during early developmental stages induces various schizophrenia-related phenotypes in mice (Figs. 1 and 3). Notably, depleting GluN2A in adult brains fails to induce most abnormalities, except those associated with negative symptoms (Fig. 2). This underscores the significance of GluN2A dysfunction during development in precipitating behavioural effects related to positive and cognitive symptoms in adult mice. The diverse timing of GluN2A dysfunction during brain development could contribute to the clinical heterogeneity observed in schizophrenia. It is crucial to acknowledge that our data alone do not conclusively support GluN2A dysfunction as the sole source of schizophrenia heterogeneity in general.

Notably, reduced PPI could serve as an important biomarker for schizophrenia, aligning with clinical findings of impaired startle habituation and PPI in patients with the disorder. Our results unmistakably show that deficits in PPI manifest when GluN2A is depleted during germline and developmental stages in both excitatory and inhibitory neurons, but not in adulthood. Furthermore, abnormal EEG patterns, including spontaneous spike and wave discharges during slow-wave sleep and a reduction in slow-wave activity and sleep quality,[56] were observed in GluN2A$^{-/-}$ mice. Collectively, these findings reinforce the idea that disruptions in GluN2A during brain development could contribute to schizophrenia-related phenotypes.

The results presented in our study suggest that early intervention may prove more effective than later intervention in addressing certain aspects of schizophrenia. Failures in drug discovery efforts aimed at enhancing NMDAR signalling to treat schizophrenia underscore the significance of this inquiry.[57–60] Nevertheless, it is evident that treatment with NMDAR inhibitors induces acute abnormalities related to schizophrenia in adults.[40] The necessity for GluN2A hypofunction during development to induce schizophrenia-related phenotypes does not necessarily preclude the possibility that boosting NMDAR signalling in adults might not reverse existing conditions with a developmental cause. Addressing this critical question is paramount, and our results advocate for testing interventions as early as possible.

It is counterintuitive that GluN2A KO on excitatory and inhibitory neurons respectively, leads to an overlapping spectrum of behavioural dysfunctions associated with schizophrenia. One possible explanation is that the overlapped behavioural dysfunction arises from impaired excitatory and inhibitory balance (E/I imbalance), triggered by dysfunction of either type of neurons. In line with our findings, recent studies have reported that E/I imbalance is a potential pathophysiological mechanism, and dysfunction in both excitatory and inhibitory neurons can both contribute to schizophrenia.[61,62]

Changes in interneurons have frequently been associated with schizophrenia.[32,63] It has been widely assumed that these changes result from cell-autonomous dysfunctions of interneurons. Experimental evidence has demonstrated that depletion of GluN1 in interneurons, not in pyramidal neurons, leads to changes in alterations in the expression of interneuron genes.[32,44–46,63] However, our study clearly demonstrates that the expression of NPY in interneurons is significantly elevated in the mPFC of NEX-Cre GluN2A cKO mice (Fig. 7j), suggesting that NMDARs in excitatory neurons could also regulate the expression of interneuron genes, likely through non-cell-autonomous mechanisms. Nevertheless, the degree of elevation in NPY expression appears to be smaller in the NEX-Cre GluN2A mPFC (Fig. 7h and j),

indicating that GluN2A in excitatory neurons only partially contributes to this effect. Overall, the distinct phenotypes observed in excitatory neuron versus inhibitory neuron GluN2A depletion indicate that GluN2A could contribute to the heterogeneity of schizophrenia through its effects on different types of neurons.

When GluN2A was specifically knocked out in smaller brain regions, such as the hippocampus and mPFC, we observed similar schizophrenia-related phenotypes (Fig. 6 and Supplementary Fig. S3). However, not all abnormalities were recapitulated in these regional GluN2A KO mice when compared with the NEX-Cre cKO or germline KO mice. It remains unclear whether GluN2A in the hippocampus or mPFC is solely responsible for some of the observed phenotypes, or if our method only partially removes GluN2A in these two brain regions.

Defects in synaptic genesis underlie schizophrenia.[64] GluN2A is expressed during the postnatal developmental stage, coinciding with the period of synaptic genesis. To investigate the potential involvement of synaptic genesis in GluN2A function, we assessed synaptic transmission in different GluN2A KO mouse strains. Surprisingly, both germline and developmental KO of GluN2A significantly enhanced excitatory synaptic transmission (Fig. 7a–d and Supplementary Fig. S6a–d). Conversely, this effect was notably absent when GluN2A was removed after development (Supplementary Fig. S6e–h). This implies that GluN2A might be critical for synaptic genesis, likely pruning, and the defects of which might lead to abnormally elevated synaptic activity and schizophrenia-related phenotypes in mice.

NPY is a neurotransmitter predominantly synthesized within GABAergic neurons.[49] Defects in the NPY system have been implicated in brain diseases including depression, anxiety, schizophrenia and trauma-induced disorders.[49,50] Our findings revealed a significant increase in NPY expression in GluN2A$^{-/-}$ mice and NEX-Cre GluN2A cKO mice (Fig. 7h and j), aligning closely with behavioural defects-associated with schizophrenia. In addition, recent single nucleus RNA-sequencing analysis also showed increased expression of a number of neuropeptides including NPY and Cort in the PFC parvalbumin (PV) and somatostatin (SST) interneurons of GluN2A$^{+/-}$ and GluN2A$^{-/-}$ mice, consistent with our observation.[65] NPY has emerged as a critical molecule in comprehending schizophrenia, supported by accumulating evidence that underscores its potential involvement, including higher NPY immunoreactivity in the CSF of patients with schizophrenia,[50] a correlation between NPY levels and social competence in schizophrenia.[49] The NPY Y2 receptor appears to be critical. Intriguingly, both its activation by agonist and genetic depletion lead to schizophrenia-related phenotypes.[66–68] These findings suggest that activation of the NPY system might underlie GluN2A KO-induced schizophrenia-related phenotypes.

Reduced startle response has been proposed to reflect a behaviour related to a reduced anxiety level.[41,69] Consistently, we observed a reduced trend in the startle response and reduced anxiety-like behaviours in GluN2A$^{-/-}$ mice (Fig. 1l). However, the vGAT GluN2A cKO mice displayed significantly reduced startle responses in the PPI test (Fig. 5k), but increased anxiety in the EPM.[34] This result suggests that reduced startle response might not always indicate reduced anxiety levels.

In summary, our study identifies the developmental stages, cell types, and brain regions in which depletion of GluN2A results in various phenotypes related to various domains of schizophrenia symptoms. These findings support the notion that GluN2A is sufficient to give rise to the heterogeneous manifestations observed in schizophrenia.

Contributors

Conceptualization, Y.C., Y.G and J.H.; Methodology, Y.L., L.M., J.E. and C.F.; Formal Analysis, Y.L., L.M., J.E. C.F; Investigation, Y.L., L.M., J.E., C.F., C.S., X.M. and T.S.; Resources, J.Y., H.J. and J.H.; Writing – Original Draft, Y.L., L.M. and Y.C.; Writing – Review & Editing, Y.L., L.M., J.E., J.H., Y.G. and Y.C.; Funding Acquisition, Y.G. and Y.C.; Supervision, Y.G. and Y.C. Both Y.L. and L.M. contributed equally. Y.L., L.M., and Y.C. had accessed and verified the underlying data. All authors have read and approved the final version of the manuscript.

Data sharing statement

The datasets used and/or analysed during the current study are available from the corresponding author on reasonable request.

Declaration of interests

Y.C. is a founder of Synphatec (Shanghai) Biopharmaceutical Technology Co., Ltd.

Acknowledgements

We thank the RIKEN BRC Animal Facility for providing the Grin2a$^{-/-}$ mice (through the National Bio-Resource Project of the MEXT, Japan) under the permission of Dr. Shigetada Nakanishi (Osaka Bioscience Institute and Kyoto University). We thank Dr. Ji Hu (Shanghai Tech University) and Dr. Zilong Qiu (Institute of Neuroscience, Chinese Academy of Sciences) for providing the vGAT-Cre and NEX-Cre mice. We thank the staff members of the Animal Facility at the National Facility for Protein Science in Shanghai (NFPS), Shanghai Advanced Research Institute, Chinese Academy of Sciences, China for providing assistance in mouse breeding and maintenance. This project received support from the Shanghai Municipal Science and Technology Major Project (Grant No. 2019SHZDZX02) awarded to Y.C. and the Natural Science Foundation of Shanghai (Grant No. 19ZR1468600 and 201409003800) awarded to G.Y.

Appendix A. Supplementary data

Supplementary data related to this article can be found at https://doi.org/10.1016/j.ebiom.2024.105045.

References

1 Sullivan PF, Kendler KS, Neale MC. Schizophrenia as a complex trait: evidence from a meta-analysis of twin studies. *Arch Gen Psychiatry*. 2003;60(12):1187–1192.
2 Kahn RS, Sommer IE, Murray RM, et al. Schizophrenia. *Nat Rev Dis Prim*. 2015;1:15067.

3 Jauhar S, Johnstone M, McKenna PJ. Schizophrenia. *Lancet*. 2022;399(10323):473–486.
4 Seaton BE, Goldstein G, Allen DN. Sources of heterogeneity in schizophrenia: the role of neuropsychological functioning. *Neuropsychol Rev*. 2001;11(1):45–67.
5 Alnæs D, Kaufmann T, van der Meer D, et al. Brain heterogeneity in schizophrenia and its association with polygenic risk. *JAMA Psychiatr*. 2019;76(7):739–748.
6 Di Biase MA, Geaghan MP, Reay WR, et al. Cell type-specific manifestations of cortical thickness heterogeneity in schizophrenia. *Mol Psychiatr*. 2022;27(4):2052–2060.
7 Creese I, Burt DR, Snyder SH. Dopamine receptor binding predicts clinical and pharmacological potencies of antischizophrenic drugs. *Science*. 1976;192(4238):481–483.
8 Moghaddam B, Javitt D. From revolution to evolution: the glutamate hypothesis of schizophrenia and its implication for treatment. *Neuropsychopharmacology*. 2012;37(1):4–15.
9 Howes OD, Kapur S. The dopamine hypothesis of schizophrenia: version III–the final common pathway. *Schizophr Bull*. 2009;35(3):549–562.
10 Howes O, McCutcheon R, Stone J. Glutamate and dopamine in schizophrenia: an update for the 21st century. *J Psychopharmacol*. 2015;29(2):97–115.
11 Uno Y, Coyle JT. Glutamate hypothesis in schizophrenia. *Psychiatr Clin Neurosci*. 2019;73(5):204–215.
12 Krystal JH, Karper LP, Seibyl JP, et al. Subanesthetic effects of the noncompetitive NMDA antagonist, ketamine, in humans. Psychotomimetic, perceptual, cognitive, and neuroendocrine responses. *Arch Gen Psychiatry*. 1994;51(3):199–214.
13 Lahti AC, Koffel B, LaPorte D, Tamminga CA. Subanesthetic doses of ketamine stimulate psychosis in schizophrenia. *Neuropsychopharmacology*. 1995;13(1):9–19.
14 Wandinger KP, Saschenbrecker S, Stoecker W, Dalmau J. Anti-NMDA-receptor encephalitis: a severe, multistage, treatable disorder presenting with psychosis. *J Neuroimmunol*. 2011;231(1–2):86–91.
15 Singh T, Poterba T, Curtis D, et al. Rare coding variants in ten genes confer substantial risk for schizophrenia. *Nature*. 2022;604(7906):509–516.
16 Trubetskoy V, Pardinas AF, Qi T, et al. Mapping genomic loci implicates genes and synaptic biology in schizophrenia. *Nature*. 2022;604(7906):502–508.
17 Paoletti P, Bellone C, Zhou Q. NMDA receptor subunit diversity: impact on receptor properties, synaptic plasticity and disease. *Nat Rev Neurosci*. 2013;14(6):383–400.
18 Mohn AR, Gainetdinov RR, Caron MG, Koller BH. Mice with reduced NMDA receptor expression display behaviors related to schizophrenia. *Cell*. 1999;98(4):427–436.
19 Duncan GE, Moy SS, Perez A, et al. Deficits in sensorimotor gating and tests of social behavior in a genetic model of reduced NMDA receptor function. *Behav Brain Res*. 2004;153(2):507–519.
20 Dzirasa K, Ramsey AJ, Takahashi DY, et al. Hyperdopaminergia and NMDA receptor hypofunction disrupt neural phase signaling. *J Neurosci*. 2009;29(25):8215–8224.
21 Halene TB, Ehrlichman RS, Liang Y, et al. Assessment of NMDA receptor NR1 subunit hypofunction in mice as a model for schizophrenia. *Genes Brain Behav*. 2009;8(7):661–675.
22 Monyer H, Burnashev N, Laurie DJ, Sakmann B, Seeburg PH. Developmental and regional expression in the rat brain and functional properties of four NMDA receptors. *Neuron*. 1994;12(3):529–540.
23 Sheng M, Cummings J, Roldan LA, Jan YN, Jan LY. Changing subunit composition of heteromeric NMDA receptors during development of rat cortex. *Nature*. 1994;368(6467):144–147.
24 von Engelhardt J, Doganci B, Jensen V, et al. Contribution of hippocampal and extra-hippocampal NR2B-containing NMDA receptors to performance on spatial learning tasks. *Neuron*. 2008;60(5):846–860.
25 Hanson JE, Weber M, Meilandt WJ, et al. GluN2B antagonism affects interneurons and leads to immediate and persistent changes in synaptic plasticity, oscillations, and behavior. *Neuropsychopharmacology*. 2013;38(7):1221–1233.
26 Higgins GA, Ballard TM, Enderlin M, Haman M, Kemp JA. Evidence for improved performance in cognitive tasks following selective NR2B NMDA receptor antagonist pre-treatment in the rat. *Psychopharmacology (Berl)*. 2005;179(1):85–98.
27 Balu DT. The NMDA receptor and schizophrenia: from pathophysiology to treatment. *Adv Pharmacol*. 2016;76:351–382.
28 Beneyto M, Meador-Woodruff JH. Lamina-specific abnormalities of NMDA receptor-associated postsynaptic protein transcripts in the prefrontal cortex in schizophrenia and bipolar disorder. *Neuropsychopharmacology*. 2008;33(9):2175–2186.
29 Catts VS, Lai YL, Weickert CS, Weickert TW, Catts SV. A quantitative review of the postmortem evidence for decreased cortical N-methyl-D-aspartate receptor expression levels in schizophrenia: how can we link molecular abnormalities to mismatch negativity deficits? *Biol Psychol*. 2016;116:57–67.
30 Carvill GL, Regan BM, Yendle SC, et al. GRIN2A mutations cause epilepsy-aphasia spectrum disorders. *Nat Genet*. 2013;45(9):1073–1076.
31 Lesca G, Rudolf G, Bruneau N, et al. GRIN2A mutations in acquired epileptic aphasia and related childhood focal epilepsies and encephalopathies with speech and language dysfunction. *Nat Genet*. 2013;45(9):1061–1066.
32 Lewis DA, Hashimoto T, Volk DW. Cortical inhibitory neurons and schizophrenia. *Nat Rev Neurosci*. 2005;6(4):312–324.
33 Kadotani H, Hirano T, Masugi M, et al. Motor discoordination results from combined gene disruption of the NMDA receptor NR2A and NR2C subunits, but not from single disruption of the NR2A or NR2C subunit. *J Neurosci*. 1996;16(24):7859–7867.
34 Su T, Lu Y, Fu C, Geng Y, Chen Y. GluN2A mediates ketamine-induced rapid antidepressant-like responses. *Nat Neurosci*. 2023;26(10):1751–1761.
35 Chen Y, Wang Y, Erturk A, et al. Activity-induced Nr4a1 regulates spine density and distribution pattern of excitatory synapses in pyramidal neurons. *Neuron*. 2014;83(2):431–443.
36 Mitra P, Bokil H. *Observed brain dynamics*. Oxford; New York: Oxford University Press; 2008.
37 Louis RP, Lee J, Stephenson R. Design and validation of a computer-based sleep-scoring algorithm. *J Neurosci Methods*. 2004;133(1–2):71–80.
38 Logesparan L, Rodriguez-Villegas E, Casson AJ. The impact of signal normalization on seizure detection using line length features. *Med Biol Eng Comput*. 2015;53(10):929–942.
39 Powell CM, Miyakawa T. Schizophrenia-relevant behavioral testing in rodent models: a uniquely human disorder? *Biol Psychiatry*. 2006;59(12):1198–1207.
40 Lee G, Zhou Y. NMDAR hypofunction animal models of schizophrenia. *Front Mol Neurosci*. 2019;12:185.
41 Boyce-Rustay JM, Holmes A. Genetic inactivation of the NMDA receptor NR2A subunit has anxiolytic- and antidepressant-like effects in mice. *Neuropsychopharmacology*. 2006;31(11):2405–2414.
42 Ludewig K, Geyer MA, Vollenweider FX. Deficits in prepulse inhibition and habituation in never-medicated, first-episode schizophrenia. *Biol Psychiatry*. 2003;54(2):121–128.
43 Biological insights from 108 schizophrenia-associated genetic loci. *Nature*. 2014;511(7510):421–427.
44 Nakazawa K, Jeevakumar V, Nakao K. Spatial and temporal boundaries of NMDA receptor hypofunction leading to schizophrenia. *NPJ Schizophr*. 2017;3:7.
45 Belforte JE, Zsiros V, Sklar ER, et al. Postnatal NMDA receptor ablation in corticolimbic interneurons confers schizophrenia-like phenotypes. *Nat Neurosci*. 2010;13(1):76–83.
46 Tatard-Leitman VM, Jutzeler CR, Suh J, et al. Pyramidal cell selective ablation of N-methyl-D-aspartate receptor 1 causes increase in cellular and network excitability. *Biol Psychiatry*. 2015;77(6):556–568.
47 Goebbels S, Bormuth I, Bode U, Hermanson O, Schwab MH, Nave KA. Genetic targeting of principal neurons in neocortex and hippocampus of NEX-Cre mice. *Genesis*. 2006;44(12):611–621.
48 Vong L, Ye C, Yang Z, Choi B, Chua S Jr, Lowell BB. Leptin action on GABAergic neurons prevents obesity and reduces inhibitory tone to POMC neurons. *Neuron*. 2011;71(1):142–154.
49 Stålberg G, Ekselius L, Lindström LH, Larhammar D, Bodén R. Neuropeptide Y, social function and long-term outcome in schizophrenia. *Schizophr Res*. 2014;156(2–3):223–227.
50 Peters J, Van Kammen DP, Gelernter J, Yao J, Shaw D. Neuropeptide Y-like immunoreactivity in schizophrenia. Relationships with clinical measures. *Schizophr Res*. 1990;3(5–6):287–294.
51 Ault DT, Werling LL. Differential modulation of NMDA-stimulated [3H]dopamine release from rat striatum by neuropeptide Y and sigma receptor ligands. *Brain Res*. 1997;760(1–2):210–217.
52 Jadi MP, Behrens MM, Sejnowski TJ. Abnormal gamma oscillations in N-Methyl-D-Aspartate receptor hypofunction models of schizophrenia. *Biol Psychiatry*. 2016;79(9):716–726.

53 Hanson JE, Ma K, Elstrott J, et al. GluN2A NMDA receptor enhancement improves brain oscillations, synchrony, and cognitive functions in dravet syndrome and alzheimer's disease models. *Cell Rep*. 2020;30(2):381–396.e4.
54 Takahashi S. Heterogeneity of schizophrenia: genetic and symptomatic factors. *Am J Med Genet B Neuropsychiatr Genet*. 2013;162b(7):648–652.
55 Chand GB, Dwyer DB, Erus G, et al. Two distinct neuroanatomical subtypes of schizophrenia revealed using machine learning. *Brain*. 2020;143(3):1027–1038.
56 Salmi M, Del Gallo F, Minlebaev M, et al. Impaired vocal communication, sleep-related discharges, and transient alteration of slow-wave sleep in developing mice lacking the GluN2A subunit of N-methyl-d-aspartate receptors. *Epilepsia*. 2019;60(7):1424–1437.
57 Balu DT, Coyle JT. The NMDA receptor 'glycine modulatory site' in schizophrenia: D-serine, glycine, and beyond. *Curr Opin Pharmacol*. 2015;20:109–115.
58 Hackos DH, Hanson JE. Diverse modes of NMDA receptor positive allosteric modulation: mechanisms and consequences. *Neuropharmacology*. 2017;112(Pt A):34–45.
59 Buchanan RW, Javitt DC, Marder SR, et al. The Cognitive and Negative Symptoms in Schizophrenia Trial (CONSIST): the efficacy of glutamatergic agents for negative symptoms and cognitive impairments. *Am J Psychiatry*. 2007;164(10):1593–1602.
60 Chang CH, Lane HY, Tseng PT, Chen SJ, Liu CY, Lin CH. Effect of N-methyl-D-aspartate-receptor-enhancing agents on cognition in patients with schizophrenia: a systematic review and meta-analysis of double-blind randomised controlled trials. *J Psychopharmacol*. 2019;33(4):436–448.
61 Gao R, Penzes P. Common mechanisms of excitatory and inhibitory imbalance in schizophrenia and autism spectrum disorders. *Curr Mol Med*. 2015;15(2):146–167.
62 Kehrer C, Maziashvili N, Dugladze T, Gloveli T. Altered excitatory-inhibitory balance in the NMDA-hypofunction model of schizophrenia. *Front Mol Neurosci*. 2008;1:6.
63 Benes FM, Berretta S. GABAergic interneurons: implications for understanding schizophrenia and bipolar disorder. *Neuropsychopharmacology*. 2001;25(1):1–27.
64 Lima Caldeira G, Peça J, Carvalho AL. New insights on synaptic dysfunction in neuropsychiatric disorders. *Curr Opin Neurobiol*. 2019;57:62–70.
65 Farsi Z, Nicolella A, Simmons SK, et al. Brain-region-specific changes in neurons and glia and dysregulation of dopamine signaling in Grin2a mutant mice. *Neuron*. 2023;111(21):3378–3396.e9.
66 Stadlbauer U, Langhans W, Meyer U. Administration of the Y2 receptor agonist PYY3-36 in mice induces multiple behavioral changes relevant to schizophrenia. *Neuropsychopharmacology*. 2013;38(12):2446–2455.
67 Karl T, Chesworth R, Duffy L, Herzog H. Schizophrenia-relevant behaviours in a genetic mouse model for Y2 deficiency. *Behav Brain Res*. 2010;207(2):434–440.
68 Méndez-Couz M, González-Pardo H, Arias JL, Conejo NM. Hippocampal neuropeptide Y(2) receptor blockade improves spatial memory retrieval and modulates limbic brain metabolism. *Neurobiol Learn Mem*. 2022;187:107561.
69 Grillon C. Models and mechanisms of anxiety: evidence from startle studies. *Psychopharmacology (Berl)*. 2008;199(3):421–437.